lated to the definition of heat transfer coefficient should be recalled. Since the expression for radiation jump is much more involved than for "conduction jump," the nature of Eq. (26) should be expected. Note that the nongrayness of gas and boundary has only parametric effects on this equation.

Large-time solution

The mathematical elaborations of Ref. 12 on the related problem are informative but hardly necessary. Clearly, an asymptotic expansion of $T(\tau,t)$ can be deduced from the behavior of $T(\tau,p)$ near its singularity with largest real part, $p = 0$ (see, for example, Ref. 16, pp. 419–420). Hence, noting, for large values of time (small values of p), that

$$[3p/(p + 4\zeta)]^{1/2} \cong (3p/4\zeta)^{1/2}(1 - p/8\zeta)$$

a first approximation to Eq. (24) may be written as

$$\bar{\psi}(\tau,p)/\psi_w = e^{-\tau^*/4(p/\zeta)^{1/2}}/p[1 + (\zeta p)^{1/2}/\lambda^*] \qquad (27)$$

The inversion of this equation (see, for example, Pair 812 of Ref. 15) is

$$\frac{\psi(\tau,t)}{\psi_w} = \operatorname{erfc}\left[\frac{\tau^*}{8(\zeta t)^{1/2}}\right] - \exp\left(\frac{\lambda^*\tau^*}{4\zeta} + \frac{\lambda^{*2}t}{\zeta}\right) \times \operatorname{erfc}\left[\frac{\tau^*}{8(\zeta t)^{1/2}} + \lambda^*\left(\frac{t}{\zeta}\right)^{1/2}\right] \qquad (28)$$

definitions of τ^* and λ^* remaining identical to those given in the small time solution. The jump in boundary temperature then follows

$$\psi(0,t)/\psi_w = 1 - \exp(\lambda^{*2}t/\zeta)\operatorname{erfc}[\lambda^*(t/\zeta)^{1/2}]$$

It is interesting to note that the approximate large time solution given by Eq. (28) is identical in form to the exact solution of the unsteady conduction in a semi-infinite solid whose ambient temperature assumes a step change. The complexity of Eq. (28) is again comparable with that of the related solutions of Ref. 12. The difference between the penetrations of radiation and conduction results in the "wavelike motion" discussed in Ref. 12. A similar behavior is not observed here because of the absence of conduction. Since the results of Ref. 12 hold for small $\mathcal{P}_0$ but not for $\mathcal{P}_0 = 0$, a direct comparison between this reference and the present study is not possible.

References

[1] Schuster, A., "Radiation Through a Foggy Atmosphere," *Astrophysical Journal*, Vol. 21, 1905, p. 1.

[2] Schwarzchild, K., "Über das Gleichgewicht der Sonnenatmosphere," *Göttinger Nachrichten*, 1906, p. 41.

[3] Wick, G. C., "Über ebene Diffusionsprobleme," *Zeitschrift für Physik*, Vol. 121, 1943, p. 702.

[4] Chandrasekhar, S., *Radiative Transfer*, Dover, New York, 1960.

[5] Goody, R. M., *Atmospheric Radiation*, Oxford University Press, London, 1964.

[6] Deissler, R. G., "Diffusion Approximation for Thermal Radiation in Gases with Jump Boundary Conditions," *Journal of Heat Transfer*, Vol. 86, 1964, p. 240.

[7] Arpaci, V. S. and Larsen, P. S., "A Thick Gas Model near Boundaries," *AIAA Journal*, Vol. 7, No. 4, April 1969, pp. 602–607.

[8] Finkleman, D., "A Note on Boundary Conditions for Use with the Differential Approximation to Radiative Transfer," *International Journal of Heat and Mass Transfer*, Vol. 12, 1969, p. 653.

[9] Traugott, S. C., "Radiative Heat Flux Potential for a Nongrey Gas," *AIAA Journal*, Vol. 4, No. 3, March 1966, pp. 541–542.

[10] Cogley, A. C., "The Radiatively Driven Discrete Acoustic Wave," *Journal of Fluid Mechanics*, Vol. 39, 1969, p. 667.

[11] Nemchinov, I. V., "Some Nonstationary Problems of Radiative Transfer," Translation TT4, 1964, Purdue Univ.

[12] Lick, W., "Transient Energy Transfer by Radiation and Conduction," *International Journal of Heat and Mass Transfer*, Vol. 8, 1965, p. 119.

[13] Cogley, A. C., Vincenti, W. G., and Gilles, S. E., "Differential Approximation for Radiative Transfer in a Nongrey Gas near Equilibrium," *AIAA Journal*, Vol. 6, No. 3, March 1968, pp. 551–553.

[14] Gilles, S. E., Cogley, A. C., and Vincenti, W. G., "A Substitute-Kernel Approximation for Radiative Transfer in a Nongrey Gas near Equilibrium, with Application to Radiative Acoustics," *International Journal of Heat and Mass Transfer*, Vol. 12, 1969, p. 445.

[15] Campbell, G. A. and Foster, R. M., *Fourier Integrals for Practical Applications*, Van Nostrand, Princeton, N. J., 1948.

[16] Arpaci, V. S., *Conduction Heat Transfer*, Addison-Wesley, Reading, Mass., 1966.

Effects of a Nonrigidly Supported Ballast on the Dynamics of a Slender Body Descending Through the Atmosphere

GERALD N. MALCOLM*

NASA Ames Research Center, Moffett Field, Calif.

Introduction

MANY atmosphere-entry bodies, particularly slender bodies, are ballasted for adequate aerodynamic static stability. The ballast typically is heavy, dense, and difficult to support in a perfectly rigid fashion under dynamic conditions. The purpose of this Note is to report some effects on the vehicle dynamics when the ballast is not rigidly supported

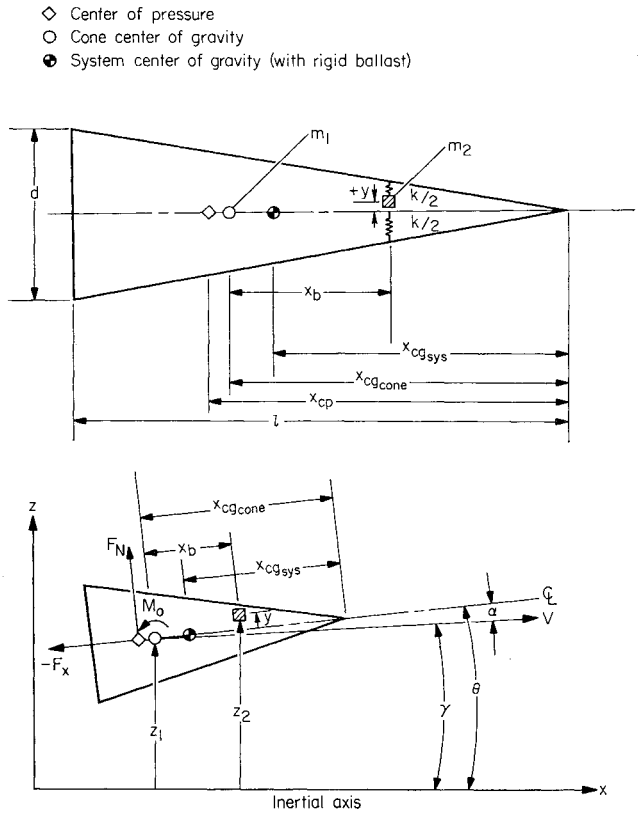

Fig. 1 Vehicle system.

Received June 17, 1970.

* Research Scientist. Member AIAA.

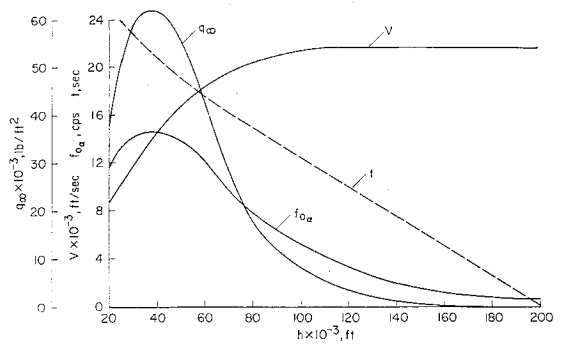

Fig. 2 Flight trajectory parameters for example case.

but oscillates as part of a coupled system with the main vehicle. A specific example—a slender cone with spring-mass system to represent the ballast arrangement—is used to illustrate some of the possible results of vehicle-ballast dynamic interaction.

Equations of Motion

The cone motion is restricted to one degree of freedom in rotation (pitch) and two degrees of freedom in translation, all in a single plane. The ballast motion is restricted to this same plane and has one-dimensional motion perpendicular to the cone axis. The system is shown in Fig. 1a where m_1 and m_2 are the masses of the cone and ballast, respectively. The centers of gravity of the cone alone, $x_{cg_{cone}}$, and of the system, $x_{cg_{sys}}$ (if the ballast were rigidly mounted), are shown with the aerodynamic center of pressure, x_{cp}. The distance of the ballast center of gravity from the reference point (i.e., the center-of-gravity position of the cone alone) is x_b. Note that $x_{cg_{sys}}$, the center of gravity of a system consisting of a vehicle with moving parts, does not remain stationary, so is not a suitable reference. The total spring constant in the ballast system is k.

This system is shown again in Fig. 1b with an inertial reference system and body-fixed aerodynamic forces F_x and F_N. The center of rotation for the aerodynamic moment, M_o, is the center of gravity of the cone alone. Shown also are angles θ, the angular position of the cone with respect to the inertial x axis, α, the angle of attack, and γ, the swerve angle.

Referring to Fig. 1b we can write the differential equations of motion. If small angles are assumed, for example,

$$\sin(\alpha) \cong \alpha, \cos(\alpha) \cong 1$$

and gravity forces are neglected, the moment and force relationships are

$$I\ddot{\theta} = M_o + (ky + b\dot{y})x_b + m_2\ddot{y}y \quad (1)$$

$$m_1\ddot{z}_1 = F_N + ky + b\dot{y} \quad (2)$$

$$m_2\ddot{z}_2 = ky - b\dot{y} \quad (3)$$

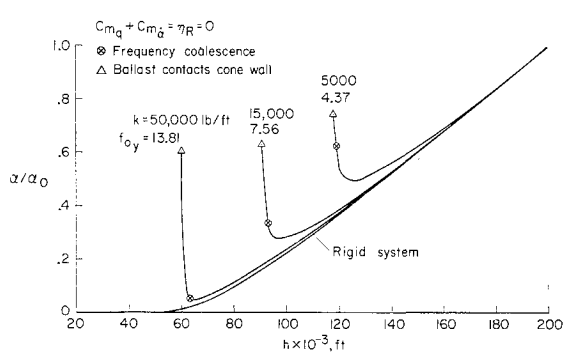

Fig. 3 Envelope of oscillatory cone motion for three different spring stiffnesses.

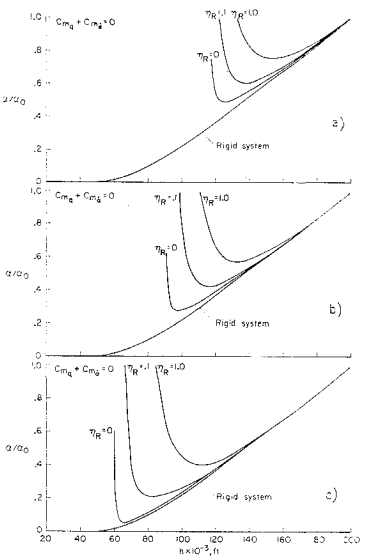

Fig. 4 Envelope of oscillatory cone motion for various ballast damping conditions. a) k = 5000 lb/ft (f_{oy} = 4.37 cps); b) k = 15,000 lb/ft (f_{oy} = 7.56 cps); c) k = 50,000 lb/ft (f_{oy} = 13.81 cps).

$$\ddot{z}_2 = \ddot{z}_1 + x_b\ddot{\theta} + \ddot{y} \quad (4)$$

where

$$M_o = C_{m_\alpha}\alpha q_\infty Ad + C_{m_q}q_\infty Ad(d/V)\dot{\theta} + C_{m_{\dot\alpha}}q_\infty Ad(d/V)\dot{\alpha}$$

$$F_N = C_{N_\alpha}\alpha q_\infty A,\ F_x = C_x q_\infty A,\ \ddot{x} = -F_x/(m_1 + m_2)$$

and I is the sum of moments of inertia of ballast and cone about transverse axes through their respective centers of gravity, b is a damping coefficient for the ballast system, q_∞ is freestream dynamic pressure, A is reference area (based on diameter), and C_{m_α}, C_{N_α}, C_x, and $C_{m_q} + C_{m_{\dot\alpha}}$ are aerodynamic coefficients for pitching-moment-curve slope, normal-force slope, axial force, and damping in pitch, respectively.

By making use of various relationships that are consistent with Fig. 1b, such as

$$\theta = \alpha + \gamma,\ \dot{z}_1 = V\gamma$$

and their derivatives, along with neglecting small terms and terms with products of aerodynamic coefficients, the equations of motion can be reduced to two simultaneous coupled differential equations.

$$\left(I + \frac{m_1m_2}{m_1 + m_2}x_b^2\right)\ddot{\alpha} - \left[q_\infty Ad\left(\frac{d}{V}\right)(CMQ)\right]\dot{\alpha} - q_\infty Ad\left(C_{m_\alpha} - \frac{m_2}{m_1 + m_2}C_{N_\alpha}\frac{x_b}{d}\right)\alpha + \frac{m_1m_2}{m_1 + m_2}x_b\ddot{y} + \frac{m_2}{m_1 + m_2}C_x q_\infty Ay = 0 \quad (5)$$

$$\ddot{y} + 2\frac{m_1 + m_2}{m_1}\eta_R\left(\frac{k}{m_2}\right)^{1/2}\dot{y} + \frac{m_1 + m_2}{m_1}\left(\frac{k}{m_2}\right)y + x_b\ddot{\alpha} + \frac{q_\infty A}{m_1}C_{N_\alpha}\left(\alpha + \frac{\dot{\alpha}}{V}x_b\right) = 0 \quad (6)$$

where

$$CMQ = C_{m_q} + C_{m_{\dot\alpha}} - \frac{C_{N_\alpha}}{m_1d^2/\{I + [m_1m_2/(m_1 + m_2)]x_b^2\}}$$

and

$$\eta_R = b/b_{crit} = b/2(km_2)^{1/2}$$

(The parameter b_{crit} is the critical damping value for the ballast system and is arbitrarily defined here as that minimum value of b that would cause the ballast to lose its oscillatory behavior if it were mounted on a stationary platform or if the cone mass were infinite.) By assuming constant q_∞ and neglecting aerodynamic and spring damping, these two equations can be solved in closed form and one can compute the oscillatory frequencies of cone and ballast, ω_1 and ω_2, respectively. When these frequencies are equal, we have "frequency coalescence." The closed-form solutions are useful in indicating trends; however, since q_∞ is time variant in actual atmosphere entry and we would normally have both aerodynamic and ballast damping, the more realistic problem is one in which the parameters vary as they would along a typical entry trajectory. Both the simplified solutions and numerical solutions to the complete problem are discussed below.

Discussion of Results

A complete study of all the parameters that affect the oscillatory motion of the vehicle was not attempted. Rather, a specific cone with a given flight trajectory, in terms of time, velocity, and dynamic-pressure variation with altitude, was used as a model. The effects of spring stiffness and spring damping in the simulated ballast system and the effects of aerodynamic damping were investigated to ascertain their influence on the oscillatory frequency and amplitude of both the ballast and the vehicle. The values used for the geometric parameters and aerodynamic coefficients are as follows (see Fig. 1):

$$d = 2.5 \text{ ft}, \; l = 7.0 \text{ ft}, \; x_{cg_{sys}} = 3.956 \text{ ft}$$

$$x_{cg_{cone}} = 4.780 \text{ ft}, \; x_{cp} = 4.928 \text{ ft}, \; x_b = 2.36 \text{ ft}$$

$$m_1 = 12.36 \text{ slugs}, \; m_2 = 6.64 \text{ slugs}, \; I = 44.44 \text{ slug-ft}^2$$

$$C_{N_\alpha} = 1.95, \; C_x = 0.075, \; C_{m_\alpha} = -0.110$$

$$C_{m_q} + C_{m_{\dot\alpha}} = 0, \; -1.5$$

The flight trajectory used for the investigation is shown in Fig. 2, where velocity, dynamic pressure, and oscillatory frequency for a rigid system (infinite spring constant) are shown for an altitude range from 200,000 to 20,000 ft. Also shown is elapsed time with $t = 0.0$ at $h = 200{,}000$ ft. The initial entry angle was taken to be $-22°$.

Oscillatory motions of both conical vehicle and ballast were obtained by integrating numerically the coupled Eqs. (5) and (6), where V and q_∞ were entered in tabular form as functions of time. The motions were started at the velocity and dynamic pressure corresponding to 200,000 ft altitude. The other initial conditions were $\alpha = 0.2$, $\dot\alpha = 0$, $y = 0$, $\dot y = 0$. The resulting motions were then studied to determine the frequency and amplitude behavior of both cone and ballast and to seek pitching divergence.

Initially, the primary oscillatory frequencies of the two motions are much different. At high altitude (where q_∞ is very small), the ballast oscillates at a primary frequency f_y near the natural frequency for a two-body system uninfluenced by any external forces or moment; that is,

$$f_y = \frac{1}{2\pi}\left(\frac{k}{m_2}\right)^{1/2}\left(\frac{m_1+m_2}{m_1}+\frac{m_2 x_b^2}{I}\right)^{1/2} = \left(\frac{m_1+m_2}{m_1}+\frac{m_2 x_b^2}{I}\right)^{1/2} f_{o_y} \quad (7)$$

where f_{o_y} is the natural frequency of a simple mass spring-mounted to a rigid platform. Initially each motion for y and α has a secondary natural frequency, which is simply the other's primary natural frequency. As the dynamic pressure increases with time, the primary oscillatory frequency f_α of the cone increases at a faster rate than would be expected for a rigid system and the primary ballast frequency decreases until the ballast and cone frequencies are the same (frequency coalescence). The motion, however, diverges sometime before frequency coalescence takes place. The amplitude of both cone and ballast increase until the ballast hits the cone. At this point describing the motion of the system becomes more complex and is beyond the scope of this investigation.

The results obtained for the effect of the ballast (with three different spring constants) on the cone motion are illustrated in Fig. 3 where the amplitude history of the cone with a nonrigid ballast is compared to one calculated for a completely rigid system. Note that for the rigid body the amplitude decreases despite the fact that $C_{m_q} + C_{m_{\dot\alpha}} = 0$ because of the increasing q_∞ with time and the damping contribution from plunging. It is apparent that the amplitude ratio is affected by the ballast long before frequency coalescence conditions occur; in fact, the motion diverges before coalescence conditions are reached. The point at which the ballast reaches the cone wall is also indicated. It can also be seen that decreasing the stiffness (k) of the ballast produces oscillatory divergence at a higher altitude (and lower q_∞). Motions obtained from closed-form solutions help to show why the coupled motion of the ballast and cone cause divergence prior to frequency coalescence.

Consider a case where the ballast and cone oscillate at a constant value of q_∞ corresponding to a value just prior to frequency coalescence. When the two bodies oscillate at nearly identical natural frequencies, a "beat frequency" is established in which the ballast motion first lags, then leads the cone motion. At frequency coalescence the ballast lags continuously. Applying this quasi-steady interpretation of the lag phenomenon to the variable q_∞ case we conclude that the divergent motion occurs somewhat before frequency coalescence is reached because of the >180° lag of the ballast that is typical of part of the beat frequency motion. Because q_∞ is continuously increasing, the beat frequency does not fully form and the ballast lags continuously until coalescence.

Figure 4 shows the effect of introducing ballast damping into the system for three different spring constants. The damping values go to a practical upper limit of $\eta_R = 1.0$ (the critical damping value for the ballast system if the ballast were attached to a rigid platform), and the effect of increased damping is to cause divergence to occur sooner in the flight. The reason is simply that if the ballast system includes damping, the ballast will lag behind the cone sooner than it would if there were no internal damping. In all cases the amplitude ratio is plotted until the ballast contacts the cone wall or the amplitude ratio increases to 1.0, whichever occurs first. The effect of adding aerodynamic damping (say, $C_{m_q} + C_{m_{\dot\alpha}} = -1.5$) is simply to delay the onset of divergence, as one would expect.

Conclusions

The effects of a nonrigidly supported ballast on the dynamic behavior of a slender body with linear aerodynamics descending through the atmosphere in planar motion have been investigated. Some important conclusions can be drawn.

The point at which frequency coalescence (ballast and cone frequencies are equal) occurs in a flight with variable dynamic pressure can be predicted accurately by means of closed-form solutions if constant values of dynamic pressure are assumed and aerodynamic and ballast damping are ignored. However, it has been shown that the amplitude of oscillations diverges before frequency coalescence is experienced. This amplitude divergence is caused by the continuous >180° phase lag of the ballast motion relative to that of the cone just prior to frequency coalescence. (Phase lag is exactly 180° at frequency coalescence.) In addition, it was found that 1) decreasing the stiffness of the ballast support causes divergence earlier in the flight (higher altitude and lower

dynamic pressure); 2) introducing damping into the ballast system (at least up to the point of critical damping for the ballast mounted on a stationary platform) produces the phase lag sooner in the flight than if there were no internal damping and therefore promotes earlier divergence of the oscillations; and 3) aerodynamic damping delays the onset of divergence.

The analysis is presented more completely, and results obtained are discussed more fully in Ref. 1.

Reference

[1] Malcolm, G. N., "The Effects of a Nonrigidly Supported Ballast on the Dynamics of a Slender Body Descending Through the Atmosphere," TN D-5622, 1970, NASA.

Characteristic Exponents for the Triangular Points in the Elliptic Restricted Problem of Three Bodies

ALI HASAN NAYFEH*
Aerotherm Corporation, Mountain View, Calif.

DANBY[3] studied the linear stability of the triangular points numerically using Floquet theory. He presented transition curves that separate the stable from the unstable orbits in the μ-e plane (μ is the ratio of the smaller primary to the sum of the masses of the two primaries, and e is the eccentricity of the primaries' orbit). These curves intersect the μ axis at μ_a and μ_0, where $\mu_a = 0.03852$ is the limiting value of μ for stable orbits in the circular case, and $\mu_0 = 0.02859$ is the value of μ such that one of the periods of motion about the triangular points is exactly twice the period of the orbit of the primaries in the circular case.

Bennett[2] obtained a first-order complicated analytical expression for the transition curves μ_0 using an analytical technique for determination of characteristic exponents. Alfriend and Rand[1] obtained second-order analytical expressions for the transition curves at μ_a and μ_0 using the method of multiple scales.[5-7] Nayfeh and Kamel[8] determined fourth-order analytical expressions for the transition curves using a perturbation technique.

In this Note, we obtain a second-order analytical expression for the characteristic exponents and the transition curves using Floquet theory[9] and a perturbation technique used by Whittaker[10] in the treatment of Mathieu equation. We use the same formulation of Refs. 1 and 8.

The first variational equation about the triangular points can be transformed into

$$x'' - 2y' - gh_2x = 0 \tag{1}$$

$$y'' + 2x' - gh_1y = 0 \tag{2}$$

where primes denote differentiation with respect to the true anomaly f of the smaller body,

$$h_{1,2} = \tfrac{3}{2}\{1 \pm [1 - 3\mu(1 - \mu)]^{1/2}\} \tag{3}$$

$$g(e,f) = (1 + e\cos f)^{-1} \tag{4}$$

It is known from Floquet theory[9] that x and y have solutions of the form

$$x,y = e^{\gamma f}[\phi(f),\psi(f)] \tag{5}$$

where ϕ and ψ are periodic with periods of 2π or 4π. Moreover, the transition curves that separate the stable from unstable domains in the μ-e plane correspond to $\gamma = 0$. In the interval $0 \leq \mu < \mu_a$, where μ_a is the critical value above which the triangular points are unstable in the case $e = 0$, the period 2π corresponds to $\mu = 0$ whereas 4π corresponds to $\mu_0 = 0.02589$. Therefore, there are transition curves that intersect the μ axis at $\mu = 0$ and μ_0. In the former case, the transition curve is the e axis. In this note, we determine the characteristic exponents near μ_0 and then deduce the transition curves.

We seek expansions for ϕ, ψ, γ, and μ of the form

$$\phi = \phi_0 + e\phi_1 + e^2\phi_2 + \ldots \tag{6}$$

$$\psi = \psi_0 + e\psi_1 + e^2\psi_3 + \ldots \tag{7}$$

$$\gamma = e\gamma_1 + e^2\gamma_2 + \ldots \tag{8}$$

$$\mu = \mu_0 + e\mu_1 + e^2\mu_2 + \ldots \tag{9}$$

Substituting Eq. (9) into Eq. (3), and expanding for small e, we get

$$h_1 = \sum_{n=0}^{\infty} a_n e^n = a_0 + ea_1 + e^2a_2 + \ldots \tag{10}$$

$$h_2 = \sum_{n=0}^{\infty} b_n e^n = b_0 + eb_1 + e^2b_2 + \ldots \tag{11}$$

where

$$a_0 = \tfrac{3}{2}\{1 + [1 - 3\mu_0(1 - \mu_0)]^{1/2}\} \tag{12}$$

$$b_0 = \tfrac{3}{2}\{1 - [1 - 3\mu_0(1 - \mu_0)]^{1/2}\} \tag{13}$$

$$b_1 = -a_1 = (9/4\kappa)(1 - 2\mu_0)\mu_1 \tag{14}$$

$$b_2 = -a_2 = (9/4\kappa)((1 - 2\mu_0)\mu_2 - \{1 - \tfrac{3}{4}[(1 - 2\mu_0)/\kappa]^2\}\mu_1^2) \tag{15}$$

$$\kappa = [1 - 3\mu_0(1 - \mu_0)]^{1/2} \tag{16}$$

On substitution of Eqs. (5-11) into Eqs. (1) and (2), expansion for small e, and equating the coefficients of e^0, e, and e^2 to zero, we obtain

order e^0

$$\phi_0'' - 2\psi_0' - b_0\phi_0 = 0 \tag{17}$$

$$\psi_0'' + 2\phi_0' - a_0\psi_0 = 0 \tag{18}$$

order e

$$\phi_1'' - 2\psi_1' - b_0\phi_1 = -2\gamma_1\phi_0' + 2\gamma_1\psi_1 + b_1\phi_0 - b_0\phi_0\cos f \tag{19}$$

$$\psi_1'' + 2\phi_1' - a_0\psi_1 = -2\gamma_1\psi_0' - 2\gamma_1\phi_0 + a_1\psi_0 - a_0\psi_0\cos f \tag{20}$$

order e^2

$$\phi_2'' - 2\psi_2' - b_0\phi_2 = -2\gamma_2(\phi_0' - \psi_0) - 2\gamma_1(\phi_1' - \psi_1) - \gamma_1^2\phi_0 + b_2\phi_0 + b_1\phi_1 + b_0\phi_0\cos^2 f - (b_1\phi_0 + b_0\phi_1)\cos f \tag{21}$$

$$\psi_2'' + 2\phi_2' - a_0\psi_2 = -2\gamma_2(\psi_0' + \phi_0) - 2\gamma_1(\psi_1' + \phi_1) - \gamma_1^2\psi_0 + a_2\psi_0 + a_1\psi_1 + a_0\psi_0\cos^2 f - (a_1\psi_0 + a_0\psi_1)\cos f \tag{22}$$

The solution of Eqs. (17) and (18) is

$$\phi_0 = A\cos\tau + B\sin\tau \tag{23}$$

$$\psi_0 = \alpha B\cos\tau - \alpha A\sin\tau \tag{24}$$

where

$$\tau = f/2, \quad \alpha = (b_0 + 1/4) + (a_0 + 1/4)^{-1} \tag{25}$$

Received June 9, 1970. It is a pleasure to acknowledge the many discussions with A. A. Kamel.

* Senior Consulting Scientist.